Research Paper

Trimethoprim and Sulfamethoxazole-Loaded Nanoparticles Coated with Chitosan for Intranasal Delivery to Treat Cerebral Toxoplasmosis

ANIELY DOS REIS TEIXEIRA[1], HEITOR DE COSTA PAULA1, ANTÔNIO LUIZ DA SILVEIRA JÚNIOR[1], AMANDA DE VASCONCELOS QUARESMA[1], RENATA TUPINAMBÁ BRANQUINHO[1], MARIA BETÂNIA DE FREITAS MARQUES[2], LEONARDO MÁXIMO CARDOSO[3] AND GISELE RODRIGUES DA SILVA[1]*

[1]School of Pharmacy, Federal University of Ouro Preto, Ouro Preto, [2]Departament of Chemistry, Federal University of Minas Gerais, Belo Horizonte, [3]Research Center in Biological Sciences-NUPEB, Federal University of Ouro Preto, Ouro Preto, Minas Gerais 35400, Brazil

Cerebral toxoplasmosis is a significant cause of morbidity and mortality, especially in immunocompromised individuals, with treatment hindered by poor drug bioavailability in the brain, systemic side effects, and relapse risk. This study aimed to develop an effective nose-to-brain therapeutic strategy using poly (ε-caprolactone) nanoparticles loaded with trimethoprim and sulfamethoxazole and coated with chitosan. Trimethoprim and sulfamethoxazole and coated with chitosan were synthesized, optimized, and coated with 0.5 % CS. Trimethoprim and sulfamethoxazole and coated with chitosan were characterized using analytical techniques, and their *in vitro* drug release and efficacy against Toxoplasma gondii-infected rat primary astrocytes were evaluated. For *in vivo* studies, trimethoprim and sulfamethoxazole and coated with chitosan were labeled with IR820, administered intranasally to mice, and their biodistribution was monitored in live animals to assess nose-to-brain delivery. TMP-SMX-NPsCS showed 174 nm, a 0.14 polydispersity index, and +31 mV zeta potential. Encapsulation efficiencies were 88.93 % for TMP and 85.23 % for SMX. FTIR and thermal analysis confirmed uniform drug dispersion and successful CS coating. *In vitro* drug release studies showed sustained release of both drugs over 24 h under simulated nasal conditions. Trimethoprim and sulfamethoxazole and coated with chitosan treatment maintained 72% cell viability compared to untreated controls. *In vivo* imaging and *ex vivo* analysis in mice confirmed brain accumulation and limited systemic distribution of IR820-labeled trimethoprim and sulfamethoxazole and coated with chitosan after intranasal administration. These findings suggest that intranasal delivery of trimethoprim and sulfamethoxazole and coated with chitosan is a promising strategy for expanding the therapeutic arsenal against cerebral toxoplasmosis by enabling direct drug delivery to the brain.

Key words: Cerebral toxoplasmosis, trimethoprim, sulfamethoxazole, chitosan, nanoparticles coated with chitosan, intranasal administration, nose-to-brain delivery

Toxoplasmosis, caused by the widespread parasite *Toxoplasma gondii* (*T. gondii*), shows varied global seroprevalence inversely related to national income: about 55 % in low, 34 % in middle, and 26 % in high-income countries[1]. While often asymptomatic in healthy individuals, it poses serious risks for immunocompromised patients, such as those with Human Immunodeficiency Virus (HIV), transplant recipients, or on immunosuppressants, due to reactivation of latent bradyzoites into tachyzoites, causing severe ocular and neurological damage[2,3]. Cerebral toxoplasmosis remains a major cause of morbidity and mortality in HIV patients, especially in low-resource areas[4-6].

Current therapies (e.g., pyrimethamine-sulfadiazine) target tachyzoites but fail to eliminate bradyzoites, leaving immunocompromised patients vulnerable to relapse[7]. Alternative regimens like trimethoprim-

***Address for correspondence**
E-mail: giselersilva@ufop.edu.br

Accepted 28 February 2026
Revised 21 November 2025
Received 19 November 2025
Indian J Pharm Sci 2026;88(1):38-50

sulfamethoxazole TMP-SMX are used in resource-limited areas or for sulfonamide-hypersensitive patients, though efficacy is reduced and severe adverse effects (e.g., Stevens-Johnson syndrome) may occur[7-9]. Critically, these drugs exhibit limited Blood-Brain Barrier (BBB) penetration, hindering the Central Nervous System (CNS) delivery[4,10].

To address these limitations, chitosan-coated poly (ε-caprolactone) nanoparticles (TMP-SMX-NPsCS) for intranasal delivery were developed. This strategy leverages the nose-to-brain pathway to bypass the BBB, enhancing CNS drug bioavailability while minimizing systemic exposure[11-13].

PCL was chosen for its high drug encapsulation and sustained release[14]. TMP and SMX were selected for their synergistic anti-*T. gondii* effects and reduced side effects[3], proving effective in both treatment and prophylaxis, especially in resource-limited or sulfa-intolerant patients[7]. Chitosan's mucoadhesive properties improve nasal retention and brain bioavailability[15]. TMP-SMX-NPsCS were optimized and characterized by Fourier Transform Infrared Spectroscopy (FTIR), thermal analysis, encapsulation efficiency, and *in vitro* drug release. Biocompatibility was tested on rat astrocytes, efficacy on infected CTX TNA2 cells, and *in vivo* studies confirmed nose-to-brain delivery for 48 h.

Therefore, it is hypothesized that TMP-SMX-NPsCS offer a promising strategy to expand the therapeutic options to treat the cerebral toxoplasmosis by enabling direct delivery of anti-Toxoplasma agents to the CNS *via* intranasal administration. This targeted approach may help overcome the limitations of conventional therapies by rapidly bypassing the BBB, reducing morbidity and mortality, preventing long-term neurological sequelae, and improving the quality of life for affected individuals.

MATERIALS AND METHODS

Materials:

Poly (ε-caprolactone) (PCL, MW ~80 000-90 000 g mol^{-1}), chitosan (CS, MW MW ~1 250 000) 50-190 kDa; degree of acetylation: 75 %-85 %), Sulfamethoxazole (SMX), Trimethoprim (TMP), penicillin, streptomycin, 3-(4,5-Dimethylthiazol-2-yl)- 2,5-Diphenyltetrazolium Bromide (MTT), polysorbate (Tween 80), chloroform, ethylic ether, and rat primary astrocyte cell line (CTX TNA2) were supplied by Sigma-Aldrich (MO, USA). Dialysis membranes (cellulose membrane, Servapor®, MW 12 000-14 000 Da) were obtained from Serva (Germany). Dulbecco's Modified Eagle Medium (DMEM), Fetal Bovine Serum (FBS), glutamine, and sodium pyruvate were purchased from Gibco (MD, United States of America (USA)). Potassium phosphate monobasic, dibasic sodium phosphate dodecahydrate, sodium hydroxide, and triethanolamine were attained from Synth (RJ, Brazil). Acetonitrile, C18 chromatographic column, and Millipore membranes were bought from Merck & Co., Inc (NJ, USA).

Development of uncoated TMP-SMX-NPs-pilot formulation:

TMP-SMX-loaded nanoparticles (TMP-SMX-NPs) were prepared by emulsification and solvent evaporation. The organic phase, containing 50 mg PCL, 3.5 mg TMP, and 17.5 mg SMX in 8 ml chloroform:ethyl ether (2:1), was stirred for 10 min and added dropwise to 6 ml aqueous phase with 1 % Tween 80. The mixture was stirred for 22 h at room temperature to evaporate solvents. NPs were collected by ultracentrifugation (14 000 g, 30 min, 8°), the supernatant discarded, and the pellet dried under vacuum for 7 d. The dried pellet was weighed and reconstituted for experiments.

Statistical experimental design:

A 2^3 factorial design was used to optimize TMP-SMX-NPs, with three factors: (A) PCL mass, (B) Tween 80 concentration, and (C) TMP and SMX masses, each at two levels (+1 high, -1 low) plus a central point (0) (Table 1). Eight formulations (1-8) and one central point (9) were prepared; formulations 1-8 in triplicate and 9 in quintuplicate (Table 2). Effects on diameter, polydispersity index, and zeta potential were analyzed by Analysis of Variance (ANOVA) at 5 % significance ($p<0.05$) using Statistical v7.0, with results shown in Pareto charts. One optimized formulation was selected and coated with chitosan. Unloaded NPs were prepared similarly without drugs.

Coating TMP-SMX-NPs with CS:

Uncoated TMP-SMX-NPs (Section 2.2) were reconstituted in 2 ml of 0.5, 1.0, or 1.5 mg/ml chitosan (CS) in 3 % (v/v) acetic acid (pH 2.35) and stirred at 1000 rpm for 30 min at 8° to form TMP-SMX-NPsCS. Unloaded NPsCS were prepared similarly

without drugs. TMP-SMX-NPs coated with 0.5 mg/ml CS were ultracentrifuge (14000 g, 30 min, 8°), supernatant removed, and pellet dried under vacuum for 7 d at room temperature. The dried pellet was weighed and reconstituted for experiments.

TABLE 1: INDEPENDENT VARIABLES: (A) PCL MASS (MG); (B) TWEEN 80 CONCENTRATION (% (W/V)); (C) TMP AND SMX MASSES COMBINED IN THE SAME FORMULATION (TMP+SMX (MG)), IN 2 LEVELS ((-1) LOW AND (+1) HIGH). THE CENTRAL POINT (ZERO - 0) REPRESENTED THE PILOT FORMULATION

Level	PCL mass (mg)	Tween 80 concentration %(w/v)	TMP+SMX mass (mg)
-1	25	0.5	0.07+0.35
0	50	1	1.0+5.0
1	75	2	3.5+17.5

TABLE 2: FACTORIAL DESIGN MATRIX: 8 UNCOATED TMP-SMX-NP FORMULATIONS ELABORATED FROM THE MODIFICATION OF INDEPENDENT VARIABLES: (A) PCL MASS (MG); (B) TWEEN 80 CONCENTRATION (% (W/V)); (C) TMP AND SMX MASSES COMBINED IN THE SAME FORMULATION (TMP+SMX (MG)), IN 2 LEVELS ((-1) LOW AND (+1) HIGH). THE FORMULATION 9* REPRESENTED THE CENTRAL POINT (0) (PILOT FORMULATION)

Formulation	PCL mass (mg)	Tween 80 concentration % (w/v)	TMP+SMX mass (mg)
1	-1	-1	-1
2	1	-1	-1
3	-1	1	-1
4	1	1	-1
5	-1	-1	1
6	1	-1	1
7	-1	1	1
8	1	1	1
9*	0	0	0

Characterization:

Determination of hydrodynamic diameter, polydispersity index, and zeta potential: Hydrodynamic diameter and polydispersity index of TMP-SMX-NPsCS and uncoated TMP-SMX-NPs were determined by Photon Correlation Spectroscopy (Malvern S4700 PCS System, Malvern Instruments, UK) using a Dynamic Light Scattering (DLS) angle of 173° at 25°. The zeta potential was measured by electrophoretic mobility by Laser Doppler Anemometry (Malvern S4700 PCS System, Malvern Instruments, UK) using 150 mV/cm potential at 25°. Analyzes were carried out on 0.5 ml of the samples diluted in 1 ml purified water. Hydrodynamic diameter, polydispersity index, and zeta potential were expressed as mean±SD for three replicates.

Encapsulation efficiency:

TMP-SMX-NPsCS and uncoated TMP-SMX-NPs were prepared as in Section 2.2. The supernatant (0.4 ml) was collected, filtered, diluted with 0.6 ml mobile phase, filtered (0.45 µm), and analyzed by HPLC. The isocratic mobile phase (triethanolamine-acetonitrile-water, 1:20:79, pH 5.9±0.1) flowed at 1 ml/min through a C18 column at 30°. Detection wavelengths were 240 nm (TMP) and 268 nm (SMX), injection volume 50 µl. TMP and SMX retention times were 3.972 and 7.994 min. Encapsulation Efficiency (EE) was calculated as the percentage difference between total drug (100 %) and non-encapsulated drug.

Fourier transform infrared spectroscopy:

TMP-SMX-NPsCS and uncoated TMP-SMX-NPs were prepared as described in Section 2.2. Infrared absorption spectra of TMP-SMX-NPsCS, uncoated TMP-SMX-NPs, and their raw materials were collected in a FTIR (MB3000, ABB Inc, Quebec, Canada). Measurements were carried out at about 2.5 mg of samples using the Attenuated Total Reflectance

(ATR) technique. Each spectrum was a result of 32 scans with a re solution of 4 cm^{-1}.

Thermal analysis: TMP-SMX-NPsCS, uncoated TMP-SMX-NPs, and unloaded NPs were prepared as described in Section 2.2. The thermal behaviour of samples was evaluated by Differential Scanning Calorimetry (DSC) and Thermogravimetry (TG). DSC curves were obtained in a DSC60 Shimadzu cell, calibrated with Indium (melting point: Tonset=156.63°, ΔHfus=28.45 $J.g^{-1}$) under dynamic nitrogen atmosphere, at 50 ml min^{-1}, heating rate of 10° min^{-1}, from 25 to 400°, in closed aluminum crucible and sample mass accurately weighted (about 1.5 mg). TG curves were obtained in a DTG60 Shimadzu under dynamic nitrogen atmosphere, at 50 mL min^{-1}, heating rate of 10° min^{-1}, from 30 to 600°, in closed aluminum crucible and sample mass accurately weighted (about 2.5 mg).

***In vitro* drug release:**

The *in vitro* release of TMP and SMX from uncoated and CS-coated NPs (n=5) was assessed using vertical diffusion cells with a dialysis membrane. Donor and receptor compartments contained PBS at pH 5.5 and 7.4, respectively, maintained at 34°. The donor received 2.5 mg NPs in 0.5 ml PBS (pH 5.5). Samples (0.5 ml) were collected at 15 min, 0.5, 1, 2, 4, 8, 12, 16, 20, and 24 h, with fresh Phosphate Buffer Solution (PBS) (pH 7.4) replaced each time. TMP and SMX release (%) was quantified by High Performance Liquid Chromatography (HPLC) (Section 2.5.2).

***In vitro* biocompatibility study:**

Astrocyte cell culture: Rat primary astrocyte cell line (CTX TNA2) was grown in DMEM supplemented with 2 mM glutamine, 1 mM sodium pyruvate, and 10 % v/v FBS in a 37° humidified atmosphere of 5 % Carbon Dioxide (CO2) and 95 % air (Thermo Scientific, USA).

Cytotoxicity: CTX TNA2 cells were seeded at 6×104 cells/well in 96-well plates and cultured for 24 h. Cells were then treated with (1) culture medium (control), (2) TMP-SMX-NPsCS, or (3) uncoated TMP-SMX-NPs at TMP+SMX concentrations of (A) 1.69+9.71 µM, (B) 1.94+11.14 µM, and (C) 2.18+12.52 µM. After 24 h incubation, wells were washed with PBS (pH 7.4) and incubated with 200 µl MTT solution (0.5 mg/ml) for 4 h at 37°, 5 % CO2. Plates were centrifuged (600 g, 5 min), medium removed, and 200 µl DMSO added for 15 min. Absorbance at 570 nm was measured. Experiments were done in triplicate with three repeats. Control absorbance was set to 100 %; sample absorbance±SD was expressed as % of control.

***In vitro* efficacy against *T. gondii*:**

Approximately 5×105 CTX TNA2 cells were seeded in 24-well plates 24 h before assay in DMEM with 2 mM glutamine, 1 mM sodium pyruvate, and 10 % FBS. Cells were infected with *T. gondii* RH tachyzoites at a 5:1 parasite-to-host ratio, centrifuged at 1000 rpm for 2 min, incubated 1 h, then washed twice with PBS. Wells received: (1) uninfected cells (control), (2) infected untreated cells, (3) TMP-SMX-NPsCS, (4) uncoated TMP-SMX-NPs, or (5) 200 µM staurosporine. TMP + SMX concentration was 1.69+9.71 µM. After 24 h incubation with 200 µl formulations, medium was replaced with 170 µl MTT (0.5 mg/mL) and 210 µl basal medium for 2 h. Formazan was dissolved in 210 µl DMSO; 100 µl transferred to 96-well plate for absorbance at 570 nm.

***In vivo* biodistribution:**

Animals: Female BALB/c mice at 6-8 w of age weighing approximately 20-30 g were obtained from the Animal Science Center (CCA) of Federal University of Ouro Preto (UFOP) and were maintained in individual cages in the Laboratory for Animal Experimentation at the School of Pharmacy at UFOP. Animals were provided with food and water ad libitum at room temperature in storage conditions with 12 h of light/dark cycles. The experimental protocol (number 5729160222) was approved by Ethics Committee for Animal Experimentation at UFOP.

***In Vivo* Imaging System (IVIS):**

Animals were anesthetized with isoflurane and intranasally administered 5 µl of: (1) IR820-labeled TMP-SMX-NPsCS, (2) IR820-labeled uncoated TMP-SMX-NPs, (3) IR820 solution, or (4) PBS control (n=6 each). TMP+SMX concentration was 1.69+9.71 µM. Biodistribution was imaged dorsally and ventrally at 0.5, 3, 6, 12, and 48 h post-administration using IVIS® LUMINA II. Fluorescence radiance ($p/s/cm^2/sr$) was recorded. Animals were euthanized under anesthesia.

***Ex vivo* organ biodistribution:** Animals were anesthetized with isoflurane and intranasally given 5 µl of (1) IR820-labeled TMP-SMX-NPsCS, (2) IR820-labeled uncoated TMP-SMX-NPs, (3) IR820 solution, or (4) PBS (n=3 each). Three hours post-administration (peak fluorescence), animals were euthanized, organs harvested, and *ex vivo* fluorescence imaged. Radiance (p/s/cm^2/sr) in ROIs was quantified using Living Image 3.2 software.

Statistical analysis:

Data were analyzed using GraphPad Prism 8 software (GraphPad, San Diego, USA). Results were expressed as means±Standard Deviation (SD) and were evaluated with one-way ANOVA. A p-value less than 0.05 was considered significant ($p<0.05$).

RESULTS AND DISCUSSION

Uncoated TMP-SMX-NPs were synthesized *via* emulsification and solvent evaporation, producing a pilot formulation with a hydrodynamic diameter of 214.9±13.2 nm, polydispersity index of 0.14±0.05, and zeta potential of -20.6±2.7 mV (Table 3). A 23 factorial design optimized these NPs by varying PCL mass, Tween 80 concentration, and TMP/SMX masses at two levels. The eight resulting formulations had diameters from 170.7 to 247.7 nm, polydispersity indices between 0.05 and 0.20, and zeta potentials from -16.6 to -20.9 mV (Table 3).

After characterizing eight uncoated TMP-SMX-NP formulations, ANOVA assessed the effects of independent variables (A: PCL mass, B: Tween 80 concentration, C: TMP-SMX mass) individually and in combination (AB, AC, BC) on physicochemical properties. Only PCL mass at the high level (+1) significantly affected diameter and polydispersity index ($p<0.05$). Tween 80, TMP-SMX mass, and their interactions showed no significant impact ($p>0.05$). P-values are summarized in Table 4, and Pareto charts illustrating effects on diameter, polydispersity, and zeta potential are in fig. 1.

TABLE 3: HYDRODYNAMIC DIAMETER (NM), POLYDISPERSITY INDEX, AND ZETA POTENTIAL (MV) OF UNCOATED TMP-SMX-NPS FROM EIGHT FORMULATIONS PREPARED FOR THE EXPERIMENTAL STATISTICAL DESIGN AND FROM THE PILOT FORMULATION (NUMBER 9)

Formulation	Hydrodynamic diameter (nm)	Polydispersity index	Zeta potential (mV)
1	179.2±4.5	0.05±0.03	-19.9±2.0
2	247.7±13.3	0.19±0.06	-20.1±0.7
3	187.2±12.7	0,09±0.02	-19.6±2.7
4	226.8±9.2	0.16±0.07	-16.6±2.2
5	179.3±10.6	0.07±0.02	-20.9±2.9
6	225.7±8.8	0.20±0.06	-19.0±1.8
7	170.7±6.9	0.08±0.02	-20.1±2.1
8	233.0±12.7	0.17±0.07	-21.0±0.8
9	214.9±13.2	0.14±0.05	-20.6±2.7

TABLE 4: 2^3 FACTORIAL DESIGN: P-VALUES FOR INDIVIDUAL INDEPENDENT VARIABLES (A) PCL MASS (MG), (B) TWEEN 80 CONCENTRATION (% (W/V)), AND (C) TMP AND SMX MASSES (MG), AND COMBINED INTERACTIONS (AB, AC, BC), ON THE HYDRODYNAMIC DIAMETER, POLYDISPERSITY INDEX, AND ZETA POTENTIAL OF UNCOATED TMP-SMX-NPS IN FORMULATIONS

Independent variables	P value		
	Hydrodynamic diameter (nm)	Polydispersity index	Zeta potential (mV)
(A)	0.0182*	0.0237*	0.0929
(B)	0.0784	0.0861	0.079
(C)	0.09	0.061	0.0798
(AB)	0.0632	0.0699	0.0792
(AC)	0.0559	0.0851	0.0824
(BC)	0.0899	0.0947	0.0925

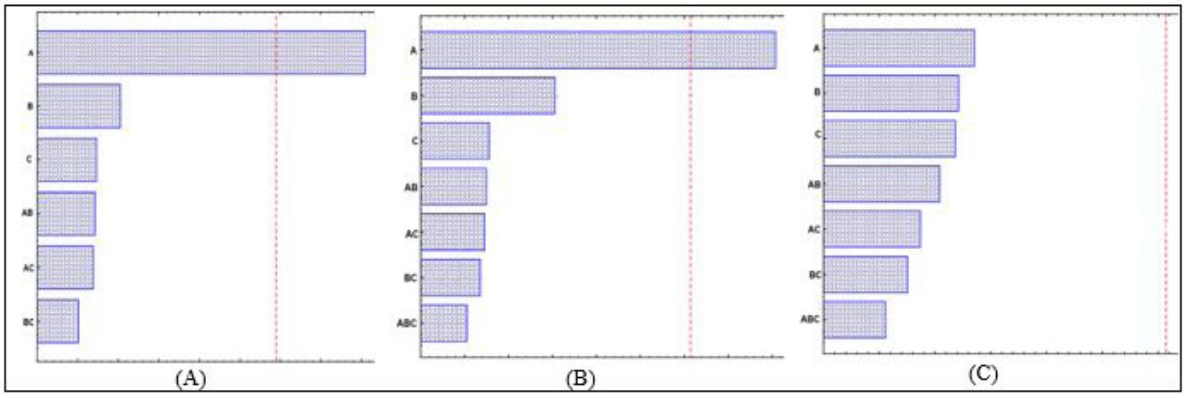

Fig. 1: Pareto chartsfrom the 2^3 factorial design: Effects of individual independent variables (A): PCL mass (mg); (B): Tween 80 concentration (% (w/v)) and (C): TMP and SMX masses (mg), and combined interactions (AB, AC, BC), on the hydrodynamic diameter (1), polydispersity index (2), and zeta potential (3) of uncoated TMP-SMX-NPs in formulations. The dotted vertical reference line represented the confidence level of 95 %

Formulation 7 was selected for CS coating due to its low PCL mass (-1), producing NPs with the smallest diameter and lowest polydispersity. Its high Tween 80 (+1) enabled high TMP and SMX loading (+1), yielding NPs with favourable properties for nose-to-brain delivery. The zeta potential was about -20 mV, slightly above the recommended -30 mV threshold[16].

Formulation 7 uncoated TMP-SMX-NPs were coated with CS at 0.5, 1.0, and 1.5 mg/ml to assess CS concentration effects. Higher CS levels increased hydrodynamic diameter and zeta potential. Coatings at 1.0 and 1.5 mg/ml also showed higher polydispersity than 0.5 mg/ml. These differences were statistically significant ($p<0.05$) (Table 5).

TABLE 5: HYDRODYNAMIC DIAMETER, POLYDISPERSITY INDEX, AND ZETA POTENTIAL OF TMP-SMX-NPS FROM FORMULATION 7 COATED WITH CS USING THREE CONCENTRATIONS OF CS

CS concentration (mg mL-1)	Hydrodynamic diameter (nm)	Polydispersity index	Zeta potential (mV)
0.5	184.2±4.8	0.14±0.02	+31.6±4.1
1.0	187.9±1.8	0.16±0.02	+34.4±3.6
1.5	190.7±2.5	0.16±0.03	+37.1±9.2

Based on these results, CS at 0.5 mg/ml was chosen to coat TMP-SMX-NPs, producing the smallest diameter, lowest polydispersity, and a zeta potential of +31 mV, indicating good stability (Melo *et al.* 2020). This formulation was used for further experiments. Encapsulation efficiencies were 88.93±2.34 % for TMP (3.11 mg) and 85.23±1.12 % for SMX (14.92 mg).

Fig. 2 shows FTIR spectra of PCL, CS, TMP, SMX, uncoated TMP-SMX-NPs, and TMP-SMX-NPsCS. PCL bands appeared at 3430, 2864, and 1722 cm^{-1} (-OH, -CH, -C=O). CS showed bands at 3422, 1648, and 1588 cm^{-1} (-OH, -NH, -C=O/-C=N). TMP bands at 3466 and 1423 cm^{-1} (-NH, -C=C), and SMX bands at 3465, 3377, 1306, and 1142 cm^{-1} (-NH, $-SO_2NH$, asymmetric/symmetric -O=S=O). TMP-SMX-NPsCS spectra featured key bands at 1722 cm^{-1} (-C=O from PCL), 3367 cm^{-1} ($-SO_2NH$ from SMX), and ~3433 cm^{-1} (-OH and -NH from PCL, CS, TMP, SMX), indicating drug dispersion and CS presence in NPs.

Fig. 3 shows DSC and TG curves of PCL, CS, TMP, SMX, uncoated TMP-SMX-NPs, and TMP-SMX-NPsCS. PCL melted at 61.02° (81.31 J/g) and was stable up to ~228°, losing 97 % mass in one step. CS lost 11.7 % moisture between 20-120° (DSC broad endotherm, 431 J/g) and decomposed from ~242° with 76 % mass loss. TMP melted at 199.47° (159.38 J/g), stable to 234°, with 2.8 % moisture loss below 120° and 85 % total mass loss by 600°, matching DrugBank specifcations[17]. SMX melted at 168.03° (126.34 J/g) without mass loss, stable to 211°, then decomposed with 86 % mass loss, consistent with USP specifications[18].

Uncoated TMP-SMX-NPs showed two DSC endothermic events: melting of PCL at ~52° and thermal decomposition at ~270°, with 100 % mass

loss. TMP-SMX-NPsCS also had melting at ~52° but decomposed at a higher temperature (~335°), likely due to CS presence, also resulting in 100 % mass loss. The higher decomposition temperature in coated NPs reflects CS's stabilizing effect. Overlapping thermal events and low drug content prevented clear distinction of each component's transitions. Results suggest drugs were dispersed in the polymer matrix and NPs were effectively CS-coated.

Fig. 4 shows *in vitro* release profiles of TMP and SMX from uncoated and CS-coated NPs. CS-coated NPs (NPsCS) released TMP progressively at 20.6 %, 49.9 %, 85.7 %, and 93.5 % over 2, 8, 16, and 24 h, while uncoated NPs released TMP faster. SMX release from NPsCS was steady (15.4 %, 38.9 %, 64.2 %, 85.2 %), but uncoated NPs released SMX more rapidly, reaching 90.3 % at 24 h. CS coating thus provides sustained drug release compared to uncoated NPs.

Fig. 5 shows CTX TNA2 cell viability after exposure to uncoated TMP-SMX-NPs and TMP-SMX-NPsCS at three TMP+SMX concentrations: (A) 1.69+9.71 µM, (B) 1.94+11.14 µM, and (C) 2.18+12.52 µM. At (A), viability was 74.19 %±4.03 % for NPsCS and 66.42 %±3.50 % for uncoated NPs. At (B), viability dropped to ~49 % (NPsCS) and 40 % (uncoated). At (C), viability further decreased to 35.62 %±4.98 % (NPsCS) and 24.70 %±4.58 % (uncoated). Cytotoxicity increased with drug concentration ($p<0.05$). Only NPsCS at the lowest concentration (A) were non-cytotoxic, exceeding the 70% viability threshold per ISO 10993-5[19].

Fig. 6 shows the *in vitro* efficacy of TMP-SMX-NPsCS and uncoated TMP-SMX-NPs against *T. gondii*-infected CTX TNA2 cells at TMP + SMX concentrations of 1.69 µM and 9.71 µM, respectively. Non-infected cells had 100 % viability, while untreated infected cells dropped to 11.28 %±4.74 %. Treatment with TMP-SMX-NPsCS and uncoated NPs increased viability to 72.04 %±6.65 % and 61.33 %±5.82 %, respectively, indicating therapeutic benefit. The increase was statistically significant ($p<0.05$), showing that NP delivery enhances TMP-SMX efficacy against *T. gondii*.

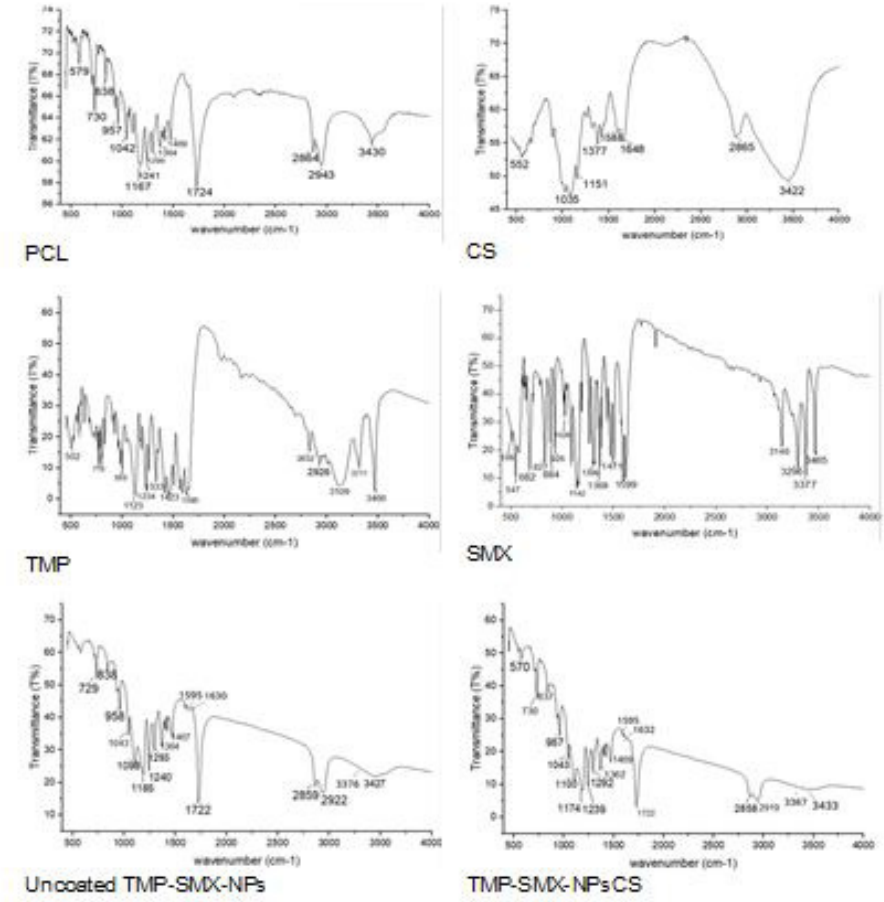

Fig. 2: FTIR spectra of PCL, CS, TMP, SMX, uncoated TMP-SMX-NPs, and TMP-SMX-NPsCS

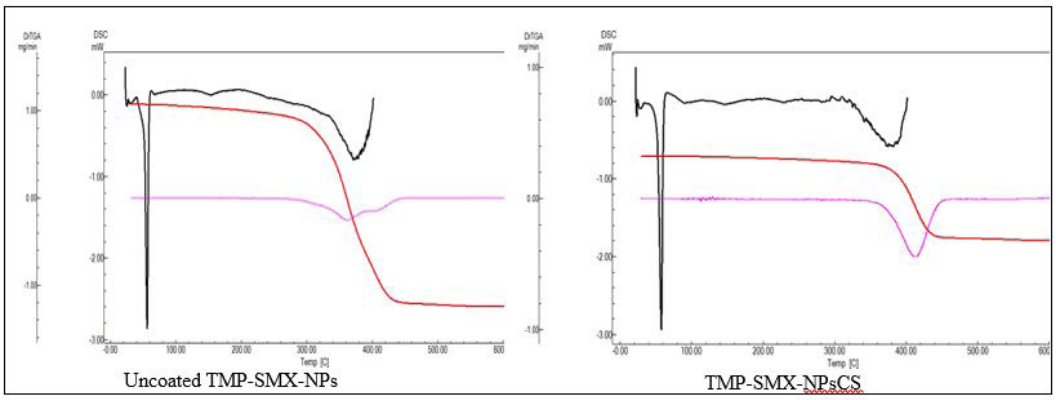

Fig. 3: DSC and TG curves of PCL, CS, TMP, SMX, uncoated TMP-SMX-NPs, and TMP-SMX-NPsCS

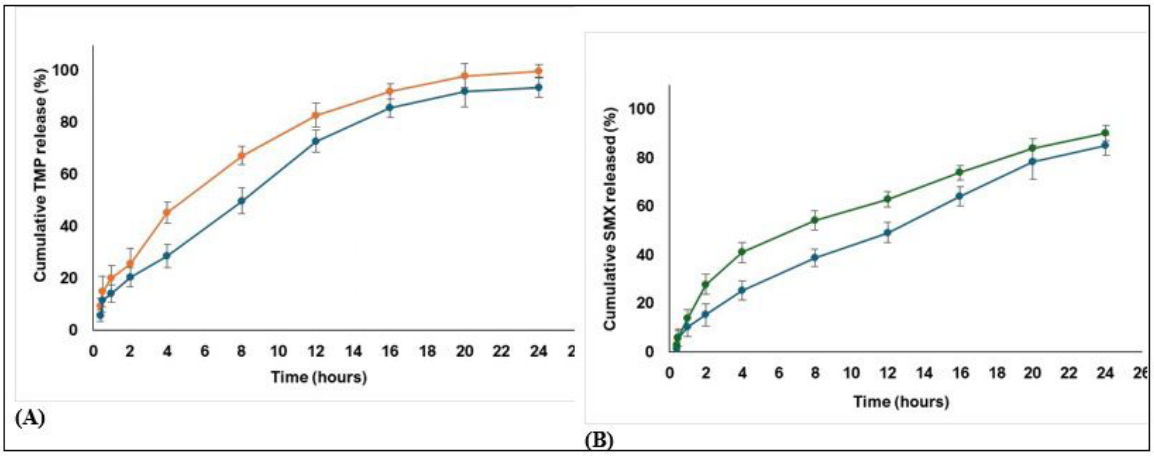

Fig. 4: *In vitro* TMP (A) and SMX (B) released from uncoated NPs and NPsCS in simulated nasal physiological conditions (PBS pH 5.5 at 34°)
Note: ( ): Uncoated TMP-NPs; ( ): TMP-NPsCS; ( ): SMX-NPsCS and ( ): Uncoated SMX-NPs

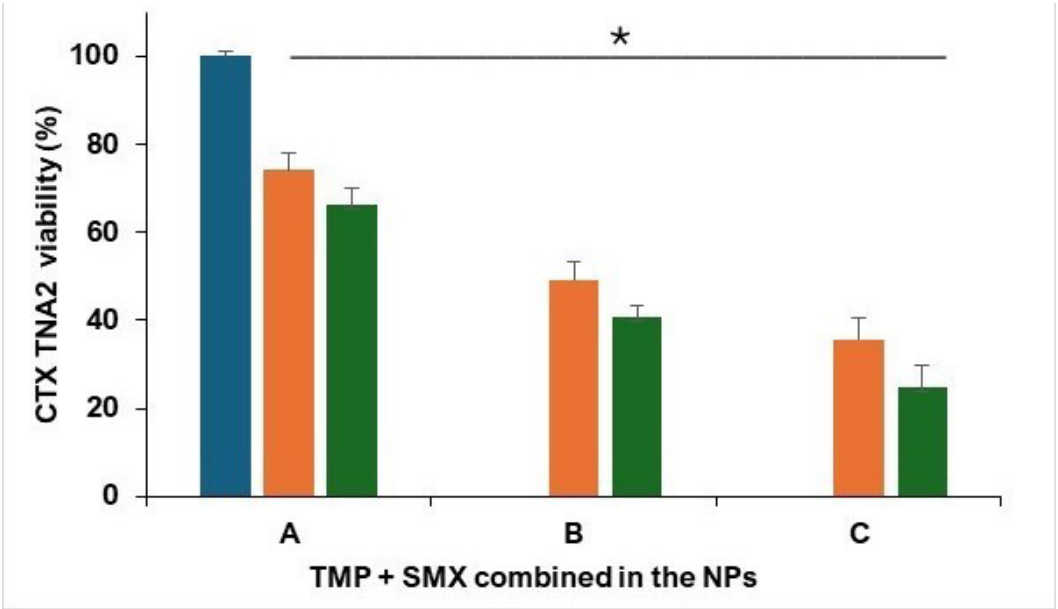

Fig. 5: Viability of CTX TNA2 cells (%) after exposure to TMP-SMX-NPsCS and uncoated TMP-SMX-NPs. The concentrations of TMP and SMX combined in the NPs reconstituted in culture medium (TMP + SMX) were as follows: (A): 1.69+9.71 µM; (B): 1.94+11.14 µM and (C): 2.18 + 12.52 µM. Data are expressed as mean±SD relative to the control, which was set at 100 % (n=10, triplicate) *p<0.05
Note: ( ): Control; ( ): TMP-SMX-NPsCS and ( ): Uncoated TMP-SMX-NPs

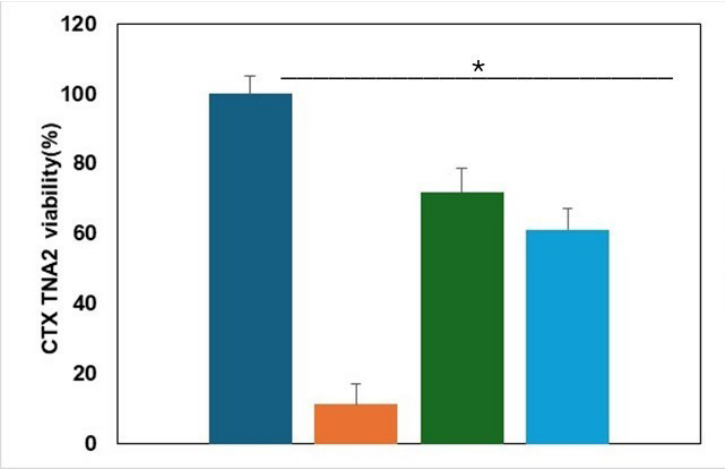

Fig. 6: Viability of CTX TNA2 cells infected by *T. gondii* (%) after exposure to TMP-SMX-NPsCS and uncoated TMP-SMX-NPs. The concentration of TMP and SMX combined in the NPs reconstituted in culture medium (TMP+SMX) was (A): 1.69+9.71 µM. Data are expressed as mean±SD relative to the non-infected CTX TNA2 cells (control group), which was set at 100 % (n=10, triplicate) *p<0.05

Note: ( ): Non-infected CTX TNA2; ( ): Untreated infected CTX TNA2; ( ):TMP-SMX-NPsCS and ( ): Uncoated TMP-SMX-NPs

The *in vivo* biodistribution of IR820-labeled uncoated TMP-SMX-NPs, IR820-labeled TMP-SMX-NPsCS, free IR820 (dissolved in PBS), and a PBS control was evaluated in healthy, live BALB/c mice at 0.5, 3, 6, 12, and 48 h post-intranasal administration. Representative *in vivo* images, obtained *via* IVIS®, were shown in fig. 7. In contrast, the labeled formulations and free IR820 displayed fluorescence signals in various regions of the animals' bodies.

For the IR820-labeled TMP-SMX-NPsCS group, the NPs accumulated in the head region within 30 min of intranasal administration, exhibiting high fluorescence intensity, as indicated by a red signal. At 3 h, peak fluorescence intensity was observed in both the head and ventral areas. By 6 h, a high fluorescence signal persisted in the head region, indicated by the continued presence of the red signal, while the signal in the ventral area notably decreased. By 48 h post-administration, moderate fluorescence intensity (green signal) persisted in the head region, while low fluorescence intensity (blue signal) in small areas was observed in the ventral region (fig. 7A). Analysis of total fluorescence intensity, quantified by radiance, over the experimental period revealed that the highest signal, equivalent to 5.07×1010 p/s/cm^2/sr, was achieved at 3 h post-intranasal administration (fig. 7B). This quantitative data corroborated the qualitative observations from the *in vivo* real-time biodistribution images.

For the IR820-labeled uncoated TMP-SMX-NPs group, the NPs were present in the head region 30 min post-administration, as evidenced by the red fluorescence signal. In addition, these NPs distributed throughout the ventral area. At 3 h, the fluorescence intensity reduced in the head area to a moderate fluorescence signal (green color) and the signal was concentrated in the ventral region. Subsequently, the fluorescence signal continually diminished throughout the animals' bodies (fig. 7C). The highest fluorescence signal, equivalent to 4.01×1010 p/s/cm^2/sr, was achieved at 3 h post-intranasal administration (fig. 7D); a value lower than that observed for the IR820-labeled TMP-SMX-NPsCS group at the same quantification time point.

Following intranasal administration of the IR820 solution, the marker was rapidly distributed to ventral organs, exhibiting a peak fluorescence intensity of 1.27×1010 p/s/cm^2/sr (fig. 7E), followed by systemic clearance (fig. 7F), contrasting with the localized brain accumulation observed with TMP-SMX-NPsCS.

As total fluorescence intensity was determined from *in vivo* real-time biodistribution imaging, with the fluorescence peak observed at 3 h post-intranasal administration of the nanosystems, a new group of animals received intranasal doses of IR820-labeled TMP-SMX-NPsCS, IR820-labeled uncoated TMP-SMX-NPs, or free IR820. At 3 h post-administration, organs-including the brain, eye, spleen, kidney, lung, heart, and liver-were harvested and imaged *ex vivo* using the IVIS® system. This approach enabled visualization of the organ-specific uptake of the labeled formulations and free IR820, and served to

validate the *in vivo* biodistribution data.

Notably, animals administered IR820-labeled TMP-SMX-NPsCS exhibited strong fluorescent emission in the brain, corroborating accumulation in the head region and indicating effective nose-to-brain delivery. In these animals, low fluorescence was detected in the kidney and liver, suggesting limited systemic distribution. In contrast, the IR820-labeled uncoated TMP-SMX-NPs group showed more pronounced systemic biodistribution, particularly in the lung, with lower accumulation in the brain. Free IR820 did not accumulate in the brain but was detected in the kidney and liver, indicating preferential accumulation

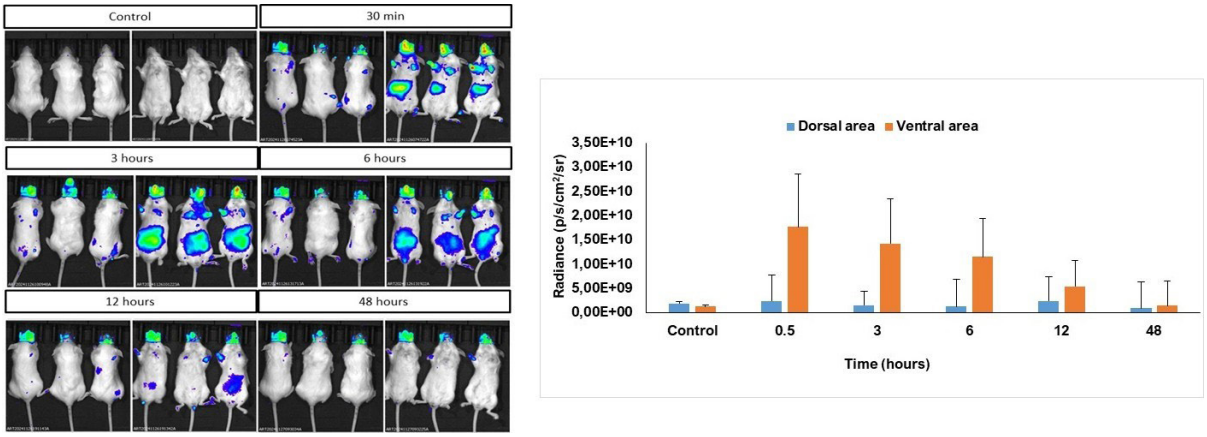

Fig. 7: Representative *in vivo* images, acquired *via* IVIS®, illustrating the biodistribution of IR820-labeled TMP-SMX-NPsCS (A), IR820-labeled uncoated TMP-SMX-NPs (C), free IR820 (dissolved in PBS) (E), and PBS control. Total fluorescence intensity, quantified as radiance (p/s/cm²/sr), in animals administered IR820-labeled TMP-SMX-NPsCS (B), IR820-labeled uncoated TMP-SMX-NPs (D), and free IR820 (dissolved in PBS) (F) at 0.5, 3, 6, 12, and 48 h post-intranasal administration

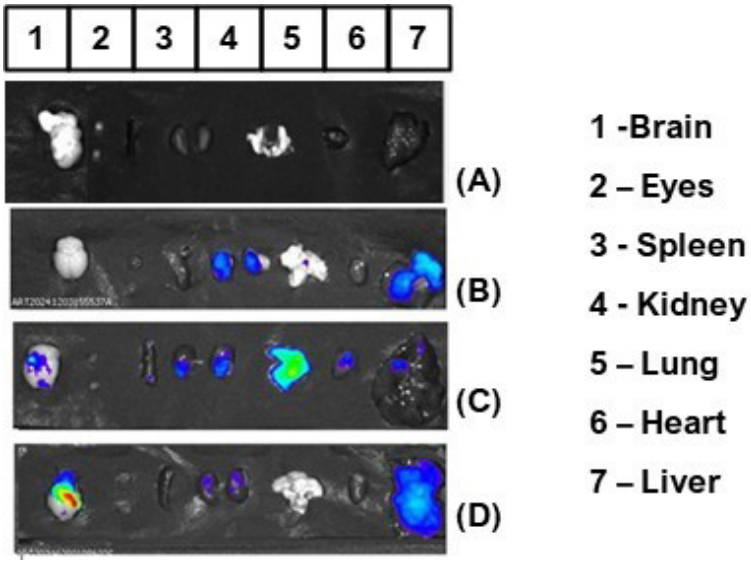

Fig. 8: Representative *ex vivo* images of the organs (brain, eye, spleen, kidney, lung, heart, liver), acquired *via* IVIS®, illustrating the biodistribution of PBS (control group) (A): Free IR820 (dissolved in PBS); (B): IR820-labeled uncoated TMP-SMX-NPs; (C): IR820-labeled TMP-SMX-NPsCS and (D): 3 h post-intranasal administration

in specific ventral regions (fig. 8).

Uncoated TMP-SMX-NPs were prepared *via* emulsification and solvent evaporation using PCL for its biocompatibility and controlled drug release. TMP and SMX were chosen for their therapeutic roles against *T. gondii*, especially in immunocompromised patients with cerebral toxoplasmosis; TMP selectively inhibits the parasite's dihydrofolate reductase, reducing severe side effects[3,7]. Tween 80, with an HLB of 15 and low critical micellar concentration, stabilized the oil-in-water colloidal system, preventing NP aggregation[20,21]. The pilot NPs had a ~215 nm diameter, which can be optimized for better nasal diffusion and CNS targeting, bypassing the BBB[22].

The pilot formulation was optimized *via* statistical design. Formulation 7 uncoated TMP-SMX-NPs had the smallest diameter (~170 nm), achieved by low

PCL mass (-1) and high Tween 80 (+1). Tween 80's acyl chains likely interacted with PCL's hydrophobic chains, reducing ester group hydration and NP size[23]. Particles ≤200 nm penetrate nasal mucus and cross olfactory pathways for CNS delivery[24]. These NPs showed a low polydispersity index (~0.08), indicating stability enhanced by Tween 80's hydrophilic surface providing steric stabilization[25]. A zeta potential of ~-20 mV added electrostatic repulsion, further stabilizing the NPs.

Uncoated TMP-SMX-NPs from formulation 7, chosen for their favorable properties, were coated with CS. The TMP-SMX-NPs-CS showed an increased hydrodynamic diameter (~184 nm), confirming CS adsorption while remaining under 200 nm, ideal for nose-to-brain delivery. The zeta potential shifted positively to ~+31 mV, reflecting cationic CS on the surface. FTIR and DSC data supported CS coating and drug dispersion within the nanosystems.

The cationic surface of CS-coated TMP-SMX-NPs enhances interaction with negatively charged nasal mucus, promoting retention by reducing mucociliary clearance[24]. This improves drug uptake by olfactory epithelial cells and transport *via* olfactory and trigeminal nerves for brain delivery[26]. Studies show that CS coating's surface and size critically affect intranasal transport, absorption, and brain drug bioavailability[6, 26, 27].

TMP-SMX-NPs-CS had a hydrodynamic diameter of ~184 nm, larger than uncoated NPs but under 200 nm, ideal for nose-to-brain delivery. The CS coating shifted zeta potential to +31 mV, reflecting its cationic surface. FTIR and DSC confirmed CS adsorption and drug dispersion. The cationic surface enhances interaction with negatively charged nasal mucus, improving retention, drug uptake by olfactory cells, and transport *via* olfactory and trigeminal nerves for brain delivery[26]. Studies emphasize that CS coating's surface and size critically affect intranasal transport, absorption, and brain bioavailability[6,26,27].

NPsCS showed controlled, gradual *in vitro* release of TMP and SMX over 24 h in simulated nasal conditions (PBS pH 5.5, 34°)[28,29]. Sustained release resulted from drug entrapment in the hydrophobic PCL matrix and the CS coating acting as a barrier, slowing diffusion compared to uncoated NPs. This prolonged release maintains therapeutic drug levels, ensuring consistent parasite suppression without frequent dosing.

Astrocytes, the main CNS glial cells, regulate metabolism, synapses, plasticity, and limit leukocyte infiltration to protect neurons[30,31,32]. In cerebral toxoplasmosis, *T. gondii* infects neurons and astrocytes, with tachyzoites preferring astrocytes due to higher replication[33,34]. Since astrocytes support parasite persistence and CNS homeostasis, they were chosen to assess SMX-TMP-NPsCS biocompatibility. The lack of astrocyte cytotoxicity suggests these nanosystems are safe for treating neuroinvasive toxoplasmosis.

TMP-SMX-NPsCS effectively targeted intracellular *T. gondii* tachyzoites in astrocytes, reducing parasite burden while maintaining 72 % cell viability-better than uncoated NPs (61 %) and untreated cells (11 %). This improved efficacy may stem from CS anchoring to astrocyte membranes *via* electrostatic interactions with anionic phospholipids, enhancing NP uptake and localized drug release[14]. The TMP and SMX synergy suppresses tachyzoite proliferation, suggesting this nanoformulation improves intracellular delivery and limits host cell damage.

IR820-labeled SMX-TMP-NPsCS were intranasally administered to assess nasal absorption and brain distribution. *In vivo* and *ex vivo* imaging showed strong brain accumulation peaking at 3 h and lasting 48 h, due to CS's mucoadhesion *via* electrostatic binding to nasal mucin, which delayed mucociliary clearance and enabled sustained diffusion and absorption through transcellular and paracellular routes[25,35]. This enhanced brain uptake and reduced systemic exposure confirmed nose-to-brain transport. Uncoated NPs showed minimal brain uptake, accumulating in lungs due to mucociliary clearance[36].

Our findings align with preclinical evidence supporting CS-coated nanocarriers for intranasal brain delivery. Gartziandia *et al.*[36] showed CS-coated lipid carriers had 2-3 times higher brain accumulation than uncoated ones, with minimal lung deposition, due to mucoadhesive charge interactions prolonging olfactory residence. Hanna *et al.*[37] reported naringin-loaded CS-NPs provided neuroprotection at a 267-fold lower dose than oral delivery by bypassing systemic circulation. Singh *et al.*[38] found glycol-CS-coated asenapine NLCs enhanced nasal retention and brain bioavailability while reducing fetal toxicity. Sharma *et al.*[39] confirmed higher brain levels with paroxetine-loaded CS-NPs versus free drug intranasally, maintaining

mucosal safety.

Ultimately, SMX-TMP-NPsCS represent a significant advancement in brain-targeted therapies for cerebral toxoplasmosis, offering rapid and enhanced bio distribution of SMX and TMP in the brain. This improved delivery is critical for effectively preventing the mortality and morbidity associated with neurological sequelae, particularly in immunocompromised patients who are most vulnerable to severe outcomes from this infection.

TMP-SMX-NPsCS were developed for targeted nose-to-brain delivery to treat cerebral toxoplasmosis. The optimized nanosystems showed favorable properties: ~184 nm size, +31 mV zeta potential, and >85 % encapsulation efficiency. Sustained drug release over 24 h was enabled by the PCL matrix and CS coating. In vitro, TMP-SMX-NPsCS maintained 72 % astrocyte viability and effectively reduced *T. gondii* infection, demonstrating biocompatibility and therapeutic specificity. *In vivo* imaging revealed rapid brain distribution peaking at 3 h post-intranasal administration, confirmed by *ex vivo* analysis, proving BBB bypass. Combining mucoadhesion, controlled release, and targeting, TMP-SMX-NPsCS offer a promising treatment option for cerebral toxoplasmosis, especially in immunocompromised patients.

Author contribution:

Conceptualization, Gisele Rodrigues Da Silva; Methodology, Aniely Dos Reis Teixeira, Heitor De Costa Paula, Antônio Luiz Da Silveira Júnior, Amanda De Vasconcelos Quaresma, Renata Tupinambá Branquinho, Maria Betânia De Freitas Marques, and Leonardo Máximo Cardoso; Validation, Gisele Rodrigues Da Silva, Aniely Dos Reis Teixeira, Amanda De Vasconcelos Quaresma, Renata Tupinambá Branquinho, and Maria Betânia De Freitas Marques; Formal Analysis, Gisele Rodrigues Da Silva, Aniely Dos Reis Teixeira; Investigation, Aniely Dos Reis Teixeira, Heitor De Costa Paula, and Antônio Luiz Da Silveira Júnior; Resources, Gisele Rodrigues Da Silva; Data Curation, Aniely Dos Reis Teixeira, Heitor De Costa Paula, Antônio Luiz Da Silveira Júnior, and Gisele Rodrigues Da Silva; Writing, Gisele Rodrigues Da Silva; Writing, Gisele Rodrigues Da Silva; Visualization, Gisele Rodrigues Da Silva; Supervision, Gisele Rodrigues Da Silva; Project Administration, Gisele Rodrigues Da Silva; Funding Acquisition, Gisele Rodrigues Da Silva

Data Availability:

Data will be made available on request.

Acknowledgements:

This research was supported by the National Council for Scientific and Technological Development (CNPq, Brazil) (304105/2024-4) and the Minas Gerais State Research Support Foundation (FAPEMIG, Brazil) (APQ-00182-22). We acknowledge FAPEMIG and the Research and Project Financing (FINEP, Brazil) for the improvements and expansion of the Animal Science Center (CCA, APQ-02511-22) at UFOP. We gratefully acknowledge the UFOP Multiuser Laboratory 1 of the Graduate Program in Pharmaceutical Sciences (CiPharma) for performing the analyses.

Conflict of interests:

The authors declared no conflict of interests.

REFERENCES

1. Wang ZD, Wang SC, Liu HH, Ma HY, Li ZY, Wei F, *et al.* Prevalence and burden of *Toxoplasma gondii* infection in HIV-infected people: A systematic review and meta-analysis. Lancet HIV 2017;4:e177-188.
2. Elsheikha HM, Marra CM, Zhu XQ. Epidemiology, pathophysiology, diagnosis, and management of cerebral toxoplasmosis. Clin Microbiol Rev 2020;34:10-128.
3. Vidal JE. HIV-related cerebral toxoplasmosis revisited: Current concepts and controversies of an old disease. J Int Assoc Provid AIDS Care 2019;18:2325958219867315.
4. Konstantinovic N, Guegan H, Stäjner T, Belaz S, Robert-Gangneux F. Treatment of toxoplasmosis: Current options and future perspectives. Food Waterborne Parasitol 2019;15:e00036.
5. Schmidt M, Sonneville R, Schnell D, Bigé N, Hamidfar R, Mongardon N, *et al.* Clinical features and outcomes in patients with disseminated toxoplasmosis admitted to intensive care: A multicenter study. Clin Infect Dis 2013;57:1535-41.
6. Gandhi S, Shastri DH, Shah J, Nair AB, Jacob S. Nasal delivery to the brain: harnessing nanoparticles for effective drug transport. Pharmaceutics 2024;16:481.
7. Simon SD. Centers for Disease Control and Prevention (CDC). InEncyclopedia of Big Data Cham: Springer International Publishing; 2022. P. 158-61.
8. Dunay IR, Gajurel K, Dhakal R, Liesenfeld O, Montoya JG. Treatment of toxoplasmosis: historical perspective, animal models, and current clinical practice. Clin Microbiol Rev 2018;31:10-128.
9. Ali M, Viqar U. Unusual Presentation of stevens-johnson syndrome induced by trimethoprim-sulfamethoxazole: A case report. Annal Punjab Med Coll 2024;18:269-271.
10. Robert-Gangneux F, Sterkers Y, Yera H, Accoceberry I, Menotti J, Cassaing S, *et al.* Molecular diagnosis of toxoplasmosis in immunocompromised patients: A 3-year multicenter retrospective study. J Clin Microbiol

2015;53:1677-84.
11. Maigler F, Ladel S, Flamm J, Gänger S, Kurpiers B, Kiderlen S, *et al.* Selective CNS targeting and distribution with a refined region-specific intranasal delivery technique *via* the olfactory mucosa. Pharmaceutics 2021;13:1904.
12. Omidian H, Gill EJ, Dey Chowdhury S, Cubeddu LX. Chitosan nanoparticles for intranasal drug delivery. Pharmaceutics 2024;16:746.
13. 13 Aderibigbe BA, Naki T. Chitosan-based nanocarriers for nose to brain delivery. Appl Sci 2019;9:2219.
14. 14. Teixeira AD, Quaresma AD, Branquinho RT, Santos SL, De Magalhaes JT, Da Silva FH, *et al.* Miconazole-loaded nanoparticles coated with hyaluronic acid to treat vulvovaginal candidiasis. Eur J Pharm Sci 2023;188:106508.
15. Aibani N, Rai R, Patel P, Cuddihy G, Wasan EK. Chitosan nanoparticles at the biological interface: Implications for drug delivery. Pharmaceutics 2021;13:1686.
16. Melo CM, Cardoso JF, Perassoli FB, de Oliveira Neto AS, Pinto LM, de Freitas Marques MB, *et al.* Amphotericin B-loaded Eudragit RL100 nanoparticles coated with hyaluronic acid for the treatment of vulvovaginal candidiasis. Carbohydrate Poly 2020;230:115608.
17. DrugBank. Trimethoprim; 2025.
18. United States Pharmacopeial Convention (USP). United States Pharmacopeia and National Formulary (USP 34–NF 29). Rockville, MD: USP; 2011.
19. International Organization for Standardization (ISO). ISO 10993-5:2009; 2009.
20. Kassem MG, Ahmed AM, Abdel-Rahman HH, Moustafa AH. Use of Span 80 and Tween 80 for blending gasoline and alcohol in spark ignition engines. Energy Rep 2019;5:221-30.
21. Cortés H, Hernández-Parra H, Bernal-Chávez SA, Prado-Audelo ML, Caballero-Florán IH, Borbolla-Jiménez FV, *et al.* Non-ionic surfactants for stabilization of polymeric nanoparticles for biomedical uses. Materials 2021;14(12):3197.
22. Xinchen Y, Jing T, Jiaoqiong G. Lipid-based nanoparticles *via* nose-to-brain delivery: A mini review. Front Cell Dev Biol 2023;11:1214450.
23. Joshi AS, Gahane A, Thakur AK. Deciphering the mechanism and structural features of polysorbate 80 during adsorption on PLGA nanoparticles by attenuated total reflectance–Fourier transform infrared spectroscopy. RSC Adv 2016;6(110):108545-57.
24. Chen Y, Zhang C, Huang Y, Ma Y, Song Q, Chen H, *et al.* Intranasal drug delivery: The interaction between nanoparticles and the nose-to-brain pathway. Adv Drug Deliv Rev 2024;207:115196.
25. de Oliveira Junior ER, Nascimento TL, Salomão MA, da Silva AC, Valadares MC, Lima EM. Increased nose-to-brain delivery of melatonin mediated by polycaprolactone nanoparticles for the treatment of glioblastoma. Pharm Res 2019;36(9):131.
26. Saha P, Kathuria H, Pandey MM. Nose-to-brain delivery of rotigotine redispersible nanosuspension: *In vitro* and *in vivo* characterization. J Drug Deliv Sci Technol 2023;79:104049.
27. Hard SA, Shivakumar HN, Redhwan MA. Development and optimization of in-situ gel containing chitosan nanoparticles for possible nose-to-brain delivery of vinpocetine. Int J Biol Macromol 2023;253:127217.
28. England RJ, Homer JJ, Knight LC, Ell SR. Nasal pH measurement: A reliable and repeatable parameter. ClinOtolaryngol Allied Sci 1999;24(1):67-8.
29. Rigaut C, Giaprakis A, Deruyver L, Goole J, Lambert P, Haut B. The air conditioning in the nose of mammals depends on their mass and on their maximal running speed. Sci Rep 2024;14(1):9053.
30. Blanchard N, Dunay IR, Schlüter D. Persistence of *Toxoplasma gondii* in the central nervous system: A fine-tuned balance between the parasite, the brain and the immune system. Parasite Immunol 2015;37(3):150-8.
31. Daneman R, Prat A. The blood–brain barrier. Cold Spring Harbor Perspectives Biol 2015;7(1):a020412.
32. Perez-Catalan NA, Doe CQ, Ackerman SD. The role of astrocyte-mediated plasticity in neural circuit development and function. Neural Devel 2021;16(1):1.
33. Halonen SK, Lyman WD, Chiu FC. Growth and development of *Toxoplasma gondii* in human neurons and astrocytes. J Neuropathol Exp Neurol 1996;55(11):1150-6.
34. Xie H, Sun H, Dong H, Dai L, Xu H, Zhang L, *et al.* Label-free quantitative proteomic analyses of mouse astrocytes provides insight into the host response mechanism at different developmental stages of Toxoplasma gondii. PLOS Negl Trop Dis 2023;17(9):e0011102.
35. Cogill SA, Lee JH, Jeon MT, Kim DG, Chang Y. Hopping the hurdle: Strategies to enhance the molecular delivery to the brain through the Blood–Brain Barrier. Cells 2024;13(10):789.
36. Gartziandia O, Herran E, Pedraz JL, Carro E, Igartua M, Hernandez RM. Chitosan coated nanostructured lipid carriers for brain delivery of proteins by intranasal administration. Colloids Surf B Biointerfaces 2015;134:304-13.
37. Hanna DM, Youshia J, Fahmy SF, George MY. Nose to brain delivery of naringin-loaded chitosan nanoparticles for potential use in oxaliplatin-induced chemobrain in rats: impact on oxidative stress, cGAS/STING and HMGB1/RAGE/TLR2/MYD88 inflammatory axes. Expert Opin Drug Deliv 2023;20(12):1859-73.
38. Singh SK, Hidau MK, Gautam S, Gupta K, Singh KP, Singh SK, *et al.* Glycol chitosan functionalized asenapine nanostructured lipid carriers for targeted brain delivery: Pharmacokinetic and teratogenic assessment. Int J Biol Macromol 2018;108:1092-100.
39. Sharma S, Gauba P, Tyagi A, Dang S. Chitosan-modified polymeric nanoparticles for the nose-to-brain drug delivery of paroxetine: An *in vitro* and *in vivo* evaluation. Nanoscale 2025;17(3):1687-702.